Self-Propelled Nanotools

Alexander A. Solovev,[†] Wang Xi,[†] David H. Gracias,[†,‡] Stefan M. Harazim,[†] Christoph Deneke,[†,§] Samuel Sanchez,[†,*] and Oliver G. Schmidt[†,⊥]

[†]Institute for Integrative Nanosciences, IFW Dresden, Helmholtzstrasse 20, D-01069 Dresden, Germany, [‡]Department of Chemical and Biomolecular Engineering, Department of Chemistry, Johns Hopkins University, Baltimore, Maryland 21218, United States, [§]Laboratório Nacional de Nanotecnologia, Rua Giuseppe Máximo Scolfaro 10000, Campinas, Brazil, and [⊥]Material Systems for Nanoelectronics, Chemnitz University of Technology, Reichenhainer Strasse 70, 09107 Chemnitz, Germany.

ABSTRACT We describe nanoscale tools in the form of autonomous and remotely guided catalytically self-propelled InGaAs/GaAs/(Cr)Pt tubes. These rolled-up tubes with diameters in the range of 280−600 nm move in hydrogen peroxide solutions with speeds as high as 180 μm s^{-1}. The effective transfer of chemical energy to translational motion has allowed these tubes to perform useful tasks such as transport of cargo. Furthermore, we observed that, while cylindrically rolled-up tubes move in a straight line, asymmetrically rolled-up tubes move in a corkscrew-like trajectory, allowing these tubes to drill and embed themselves into biomaterials. Our observations suggest that shape and asymmetry can be utilized to direct the motion of catalytic nanotubes and enable mechanized functions at the nanoscale.

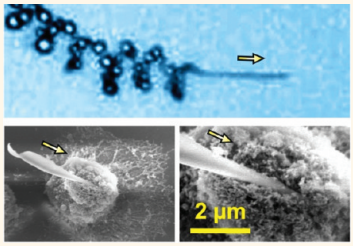

KEYWORDS: self-propulsion · nanofabrication · microjets · micromachines · catalytic motor · cell

The mimicry of mechanized macroscale functions at the nanoscale is important for nanomanufacturing and nanorobotics.[1,2] However, even simple macroscopic tasks are extremely challenging at these small size scales since it is hard to achieve and control nanoscale actuation reproducibly, reversibly, and especially in a wireless manner. Catalytically constituted micro- and nanostructures can accelerate the decomposition of hydrogen peroxide and enable the self-propulsion of micro- and nanomotors,[3−15] pumping of fluids,[16−18] and transport of colloidal particles.[19,20] It is noteworthy that versatile methods to roll up nanomembranes into functional tubes have been previously demonstrated.[21−25] Among these methods, roll-up technologies on sacrificial polymer layers have allowed the development of catalytically powered microjets[26−29] for a variety of applications including the assembly of microcargo,[30,31] capture and delivery of cells,[32,33] and the biosensing of nucleic acids.[34] Here, we fabricate catalytic tubes with diameters in the submicrometer range and investigate control over their catalytic motion.[35,36] Furthermore, we discovered that the asymmetry in the shape of the rolled-up nanotubes was important in determining their trajectory during self-propulsion and could be utilized to enable functional nanotools. The use of rolled-up tubes as nanomechanical tools, such as nanodrillers, was hypothesized over 10 years ago;[21] here, we provide the proof-of-concept of their realization.

We utilized molecular beam epitaxy (MBE) to deposit thin films of InGaAs/GaAs on sacrificial AlAs layers and bulk GaAs substrate. Considerable strain in such heteroepitaxial layers causes them to roll up into tubes with nanoscale diameters upon release from the substrate, as previously demonstrated.[37,38] In order to create self-propelled tubes, it was necessary to deposit a catalytically active platinum (Pt) layer. Even with this Pt layer, we observed that the strain in the MBE membranes was high enough so that catalytic nanotubes with diameters approximately 20 times smaller than previously reported rolled-up catalytic microjets[26,30] and half the size of the recently designed nanojets could be formed.[35] Consequently, we are reporting here the smallest man-made catalytic jet engines. Using these smaller tubes, we address several important questions. Can nanotubes overcome Brownian diffusion and move along a specific trajectory? Can the shape be utilized to alter their trajectories and as a result permit new functionalities? Can the power derived from such motion be used to perform useful tasks?

RESULTS AND DISCUSSION

To create catalytically active roll-up tubes, the successive growth of the sacrificial AlAs layer (20 nm) and the strained $In_{0.33}Ga_{0.67}As$/GaAs bilayer (3/3 nm) by MBE on a GaAs (001) substrate was followed by magnetron sputtering of different thicknesses of Pt layers. After the deposition of metals, we

* Address correspondence to s.sanchez@ifw-dresden.de.

Received for review December 6, 2011 and accepted January 10, 2012.

Published online January 10, 2012
10.1021/nn204762w

defined trenches for under-etching by scratching the samples. The selective etching of the AlAs layer was achieved using an 8.3% (v/v) HF solution for 30 s, which induced the roll-up process by strain relaxation.

We fabricated samples with different thicknesses of Pt layers from 0.5 to 2 nm and observed that a thicker Pt film leads to an increase in the diameter of the nanotubes from 280 up to 600 nm (Figure 1). We attribute this increase to the increase in the overall layer thickness, as has been discussed before.[38−40] The fabrication process is depicted in the lower inset of Figure 1 and Figure S1 in Supporting Information, showing the roll-up of the heteroepitaxially grown InGaAs/GaAs/Pt nanomembranes. The upper inset of Figure 1 shows a focused ion beam (FIB) cut SEM image of a cross section of an individual nanotube consisting of InGaAs/GaAs/Pt (3/3/0.5 nm) films.

In order to enhance the stability and mechanical rigidity of the tubes for reproducible nanotools, Cr (1 nm) as an additional adhesion layer was sandwiched between the InGaAs and Pt layers. The rolled-up thin film stack of InGaAs/GaAs/Cr/Pt (3/3/1/1 nm) had an average tube diameter of 600 nm. This number is similar to the diameter achieved when 2 nm of Pt is deposited in a thin film system of InGaAs/GaAs/Pt, as can be seen in Figure 1.

Cylindrical or asymmetrically rolled tubes can be obtained by scratching the thin films in different directions.[41] Figure 2A shows an SEM image of an InGaAs/GaAs/Cr/Pt nanotube with a slightly conical-like geometry of 10 μm length.

Platinum-coated rolled-up tubes move autonomously as nanojets when they are immersed in a solution of hydrogen peroxide (H_2O_2). The catalytic nanojets are powered by the decomposition of H_2O_2 into molecular oxygen which accumulates in the small cavity and eventually gets released from one end of the nanotube as visible bubbles (Figure 2B−D). Figure 2B−D illustrates the direction and speed of InGaAs/GaAs/Cr/Pt (3/3/1/1 nm) nanojets immersed in different concentrations of peroxide fuel. The depicted nanojets move at speeds of 12, 84, and 110 μm s^{-1} for 6, 16, and 20% v/v H_2O_2, correspondingly (corresponding videos are available in Supporting Information). These results demonstrate that bubble-driven catalytic nanojets can indeed overcome Brownian diffusion as well as the high viscous forces of the fluid at low Reynolds numbers.[42] To reduce the high surface tension inside the small tubes, 10% v/v of surfactant was added into the fuel solution.[43] Since at 20% v/v H_2O_2 the nanojets acquire high speeds and yet controllable directionality, we selected those fuel conditions as ideal to demonstrate the capabilities of these jets as nanotools.

While a few tubes rolled up into cylinders (Figure 3A), the vast majority of tubes rolled up at an angle, mainly due to the substrate orientation since layers favor rolling along the InGaAs ⟨100⟩ direction.[44] As a result,

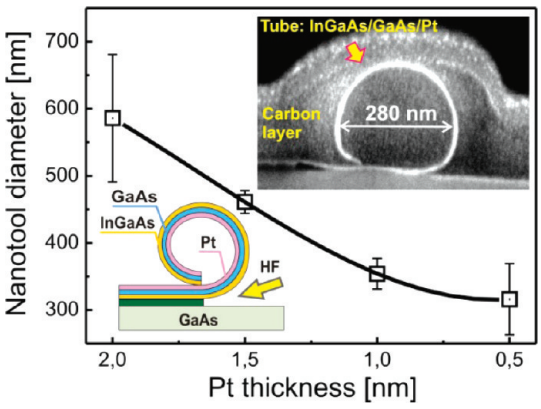

Figure 1. Scalability of the diameter of rolled-up nanotubes consisting of hybrid heteroepitaxial catalytic InGaAs (3 nm)/GaAs (3 nm)/Pt thin films. Bottom inset shows the rolled-up fabrication process by selective under-etching of the sacrificial AlAs (20 nm) layer. Top inset depicts a SEM image containing a focused ion beam (FIB) cut of an individual tube composed of InGaAs/GaAs/Pt (0.5 nm).

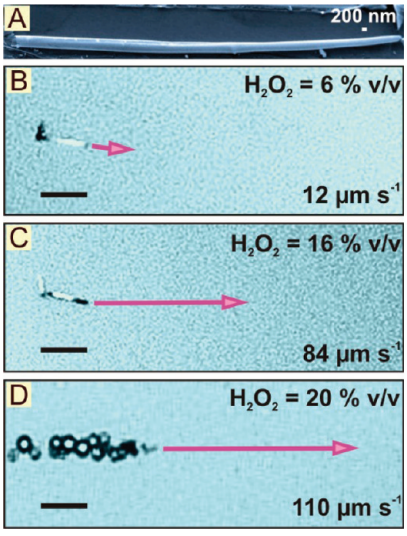

Figure 2. Motion and speeds of cylindrical catalytic rolled-up nanotubes (nanojets) in different concentrations of fuel solution. (A) SEM image of a InGaAs/GaAs/Cr/Pt (3/3/1/1 nm) nanotube with an average diameter of 600 nm. (B−D) Optical microscopy images of catalytic nanojets self-propelled in 6, 16, and 20% v/v H_2O_2 recorded during 1 s. Arrows shows the velocity magnitude at different fuel conditions. Scale bar in B and C is 15 μm and in D is 30 μm.

many of the fabricated nanotubes present a sharp tip clearly seen in Figure 3A(b,c). The release of bubbles from these rolled-up structures is asymmetric in nature, thus the catalytic nanojets move in curved trajectories (Figure 3B(b,c).[26] As a comparison, a nanojet (a) which has a straight opening self-propels linearly at 50 μm s^{-1} during 2.2 s (video 1 in Supporting Information), whereas nanojet (b) moves in a circular trajectory at speed of 63 μm s^{-1} during 3 s (video 2 in Supporting Information). Nanojet (c) containing a sharper tip moves in circular trajectories with a larger radius at a speed of 68 μm s^{-1}, during 5.2 s, and at the same time,

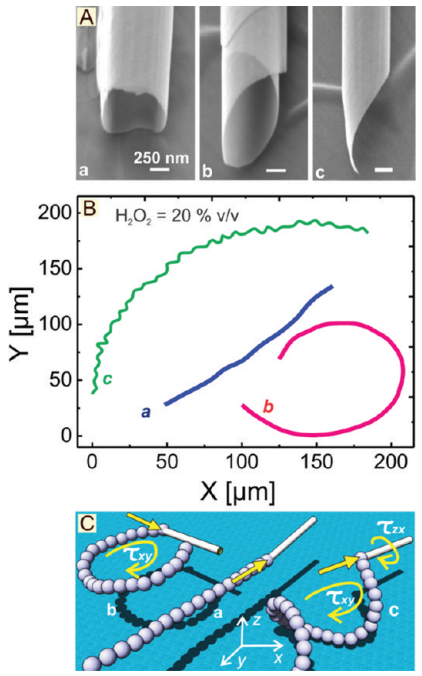

Figure 3. SEM images of rolled-up nanotubes with cylindrical and asymmetric geometries and their autonomous trajectories in 20% v/v H_2O_2 and 10% v/v surfactant. (A) SEM images of rolled-up InGaAs/Cr/Pt layers forming (a) straight cylindrical opening and (b,c) asymmetric "sharp tip" like structures. (B) Tracked trajectories of self-propelled nanotools following (a) straight, (b) circular, and (c) corkscrew-like trajectories. (C) Schematic of the trajectories with forces represented by straight yellow arrows and torques represented by circular yellow arrows.

it performs a corkscrew movement (video 3 in Supporting Information). To achieve that specific type of motion, the front end of the nanojet (c) propagates in a straight line along its long axis of symmetry while the back end of the tube performs a helix-like motion. The screw-like motion is observed only for this type of nanojets (Figure 3A(c)) and to our knowledge has never been reported either for previous rolled-up microtubular jets or for nanowire-based nanomotors.[26,30]

Figure 3C shows a schematic of the nanotools' (a) circular, (b) straight, and (c) screw-like motions. Straight arrows indicate the direction of motive force, and circular arrows show torques (τ) acting on the nanojets. The magnitude of torques depends on the driving force, the length of the lever arm, and the angle between the driving force vector and the lever arm. In the case of straight motion (nanojet (a)), the driving force acts along the long axis of symmetry, and it propels the tube in a straight line. In contrast, the origin of a torque in the $z-x$ plane (τ_{zx}) leads to a circular motion, shown in Figure 3C(b). If an additional torque (τ_{zx}) is present due to a further asymmetry at the edge of the nanotube, it can rotate the tube around its long axis and consequently lead to a corkscrew-like motion, shown in Figure 3C(c).

In order to serve as practical tools, guidance from afar could also be achieved by incorporation of a ferromagnetic layer. The deposition of a thin iron (Fe, 10 nm) layer on the top of the rolled-up tubes allowed us to steer the nanojets using a small external magnet placed underneath the working solution. Figure 4A demonstrates the remote magnetic control over the directionality of the motion of the self-propelled nanotools as reported previously for microjet engines (video 4 in Supporting Information).[30] Yellow arrows indicate the direction of nanojet propulsion, whereas white arrows show the direction of the external magnetic field (B). It is clear that a small change in the direction of the magnetic field is enough to alter the direction of the nanojets.

We exploited the capabilities of the nanotools as shuttles of yeast cells. Figure 4B illustrates the pick-up, transport, and delivery of multiple yeast cells by a catalytic nanotool in 20% v/v H_2O_2 (see videos 5–8 in Supporting Information). In the absence of attached cells, the nanotool propels within a region crowded with yeast cells at a speed of 125 μm s^{-1}. The nanotool could be guided to specific cells to be loaded (Figure 5B central panel); when loaded with three yeast cells, the tool decelerated down to a speed of 25 μm s^{-1}. It is noteworthy that, even though the nanotool has a length of 10 μm, a dimension similar to the diameter of the three transported cells, it moves at 2.5 body lengths s^{-1} while transporting the cells, illustrating the high power output of the catalytic nanojets. Since we did not utilize any antibodies, we believe that the cells were attached to the outer surface of the nanotool by van der Waals type interactions. The loaded cells were transported over a period of 25 s from a "crowded" area to a "clean" area (videos 7 and 8 in Supporting Information), enabling the transport of cells in solution by self-propelled and remotely controlled nanotools. The continuous rotation of the nanotool and the drag force weakens the attachment of the cells to the tube, so that they are eventually released. We observed that the release of the cells leads to an acceleration of the nanotool reaching speeds of about 180 μm s^{-1} (video 8 in Supporting Information). Note that this speed is higher than the initial speed in the crowded area, where the nanotool collided with several yeast cells, slightly reducing its velocity. Although the transport of cells by larger catalytic microjets was previously reported by our group[32] and Wang's group,[33] the jets utilized here are much smaller and yet powerful enough to transport cells.

We also exploited the corkscrew propulsion (video 9 in Supporting Information) of the nanojets to drill into biomaterials such as those constituting HeLa cells, which are an immortal cell line derived from cervical cancer. It should be noted that we utilized paraformaldehyde to fix the cells prior to the drilling experiments for two reasons: (a) we wanted to remove the influence

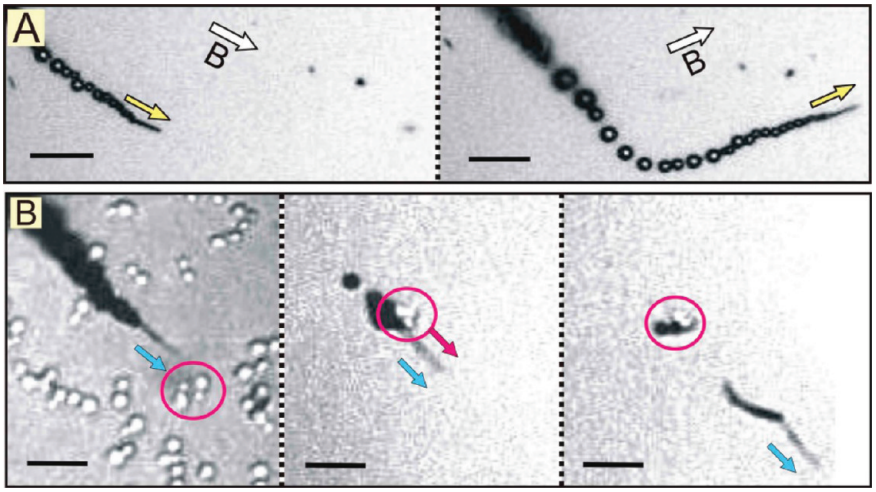

Figure 4. Remote magnetic guidance of InGaAs/GaAs/Pt nanotools. These nanojets were sputtered with a 10 nm thick layer of Fe after rolling-up, to enable magnetic guidance. (A) Image sequences showing that the nanotools are aligned in the direction of the external magnetic field. (B) Image sequences illustrating the use of self-propelled nanotools for loading, transport, and delivery of multiple yeast cells (videos 4–8 in Supporting Information). Scale bars in A and B correspond to 15 and 10 μm.

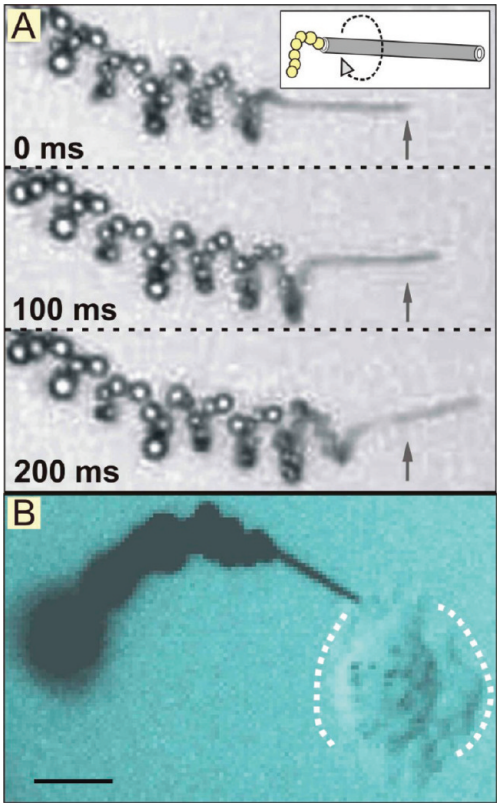

Figure 5. (A) Autonomous corkscrew-like motion of a single InGaAs/GaAs/Cr/Pt (3/3/1/1 nm) rolled-up nanojet. Arrows indicate relative motion of the nanojet between panels, and the schematic inset shows the type of motion (representative videos 3 and 9 are available in Supporting Information). (B) Optical microscopy image of an active nanotool drilling into a cross-linked biomaterial—a paraformaldehyde-fixed HeLa cell. Scale bar = 10 μm (multiple examples are available in videos 10–20 in Supporting Information).

of any chemically induced deformation of the cell during drilling in the H_2O_2 fuel; (b) these fixed cells represent a cross-linked version of a realistic cellular biomaterial, so we rationalized that, if the nanotools could generate enough force to drill into fixed cells, they would likely have more than enough force to drill into un-cross-linked cells. The type of motion needed for drilling is clearly shown in Figure 5 by optical microscope sequences of an individual nanojet which self-propels in a screw-like motion during 200 ms at a rotational frequency of 10 Hz (fuel composition: 20% v/v H_2O_2, 10% v/v surfactant). Straight arrows in the images indicate the linear displacement of the nanojet during the studied time. The inset of Figure 5A depicts a schematic of the rotation of the nanojet during translation. The optical image in Figure 5B displays a single nanotool which self-propels and embeds itself into a fixed HeLa cell (videos 10–20 in the Supporting Information show several self-propelled nanotools drilling into HeLa cells). Once the cellular boundary is reached, the nanotools stick to it and start drilling the cellular biomaterial over several minutes.

In order to gain insight into the drilling phenomena, we performed SEM using a secondary (Figure 6A,C) and backscatter (Figure 6B,D) detector which shows individual nanotools drilled into HeLa cells. The contrast in the backscatter images of Figure 6B,D is due to different atomic masses and allows us to clearly differentiate between the metallic tubes and the paraformaldehyde-fixed cells. They show that the metallic nanotools were indeed embedded into these fixed HeLa cells. The yellow arrows indicate an initial direction of nanotools drilling into the cells. We also observed this drilling *via* optical microscopy and observed that, once the nanotools reach the fixed cells, they insert a repetitive motion at a frequency above 40 Hz for the studied fuel conditions. Since a smooth rotational motion was sometimes impeded by the roughness of the object surface, we also observed a translational or impulse motion. Subsequently, once bound to the target cell,

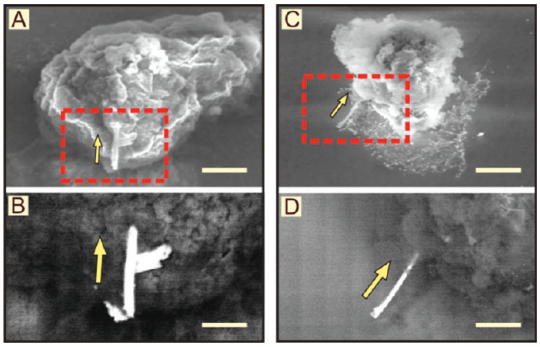

Figure 6. Rolled-up nanotool drillers. (A–C) Representative secondary electron SEM images of tubular nanotools which were autonomously embedded into a biomaterial (fixed HeLa cells). (B–D) Corresponding backscattered SEM images showing the bright contrast of the embedded nanotool compared to the soft cellular material.

we observed that each nanotool asserted this repetitive force over 2000 times a minute, which facilitated their penetration inside the fixed cell.

CONCLUSIONS

In summary, we have demonstrated the application of self-propelled catalytic nanojets fabricated by the roll-up of nanofilms deposited by molecular beam epitaxy. MBE growth of ultrathin heteroepitaxial layers allows the reduction of the tube diameter down to 280 nm, representing the smallest jet engine reported to date. The particular asymmetry of the tubular structures provides a screw-like motion which was employed for drilling into fixed cells. When a ferromagnetic layer was deposited on top of the rolled-up nanojets, an additional remote control over the motion of such nanotools enabled their directed guidance. Despite the small size, the nanotools are able to pick up and transport multiple yeast cells to desired targets. Although the fuel employed for self-propulsion is still toxic to sustain viable mammalian cellular functions, alternative mechanisms of powered motion[45–47] and working conditions foresee the use of this concept in diverse applications such as biomedical engineering, biosensing, and biophysics. Similar to other micro- and nanomotors, the propulsion nanotools may be directed by other sources such as light,[48] chemical,[49] or electrochemical stimuli.[50] While hydrogen peroxide may be acceptable for applications in nanomanufacturing and nanorobotics, biocompatible fuels need to be developed for live-cell applications. Nonetheless, due to the reduced dimensions but yet the high propulsion power, our results suggest strategies of using shape, size, and asymmetry of catalytic nanostructures as tools to realize mechanized functions at the nanoscale.

METHODS

Culturing of HeLa Cells. Before culturing HeLa cells on glass coverslips, the glass coverslips were sterilized by exposure to oxygen plasma for approximately 30 min. To ensure the attachment of cells, the slips were modified by phosphonic acids according to the protocol previously reported (*J. Am. Chem. Soc.* **1994**, *116*, 1737 and *Inorg. Chem.* **1994**, *33*, 5050). Briefly, the glass coverslips were immersed in 50 μM 11-phosphonoundecanoic acid in toluene for 12 h, then rinsed with toluene and dried at 90 °C. The fibronectin was covalently attached to phosphonic acid functionalized glass coverslips by activation of the –COOH group using EDC and NHS coupling agents. Phosphonic acid modified slips were dispersed in 1 mL of PBS containing 0.02 M EDC and 0.01 M NHS for 2 h to activate the –COOH groups. Twenty microliters of fibronectin solution (1 mg mL^{-1}) was then added to the –COOH-activated coverslip solution and left overnight at 37 °C. The activated –COOH group bound with the $-NH_3$ group of fibronectin, resulting in the formation of a covalent CO–NH amide bond. HeLa cells were dissociated by treating with trypsin (0.25%, 5 min, 37 °C), then diluted in DMEM/10% FBS supplemented with 0.5 mM L-glutamine and 1% penicillin/streptomycin and plated onto the coverslips at low density (10^4 cells cm^{-2}). The samples were flooded with freshly made medium and incubated for 24 h to allow the cell spreading. After that, the cell culture was briefly fixed in 2% paraformaldehyde for 20 min and immersed into nanotube working solution (20% peroxide and 10% common soap) for the drilling experiment.

In the transporting experiment, budding yeast cells (bakery yeast) are used. Budding yeast cells were culture in YPD medium (casein, enzymatically digested 20 g L^{-1}, yeast extract 10 g L^{-1}, glucose 20 g L^{-1}, pH value 6.5 ± 0.2, Carl Roth GmbH + Co. KG) overnight at 28 °C. Yeast cells were then transferred into nanotube working solution for the transport and delivery experiment. The concentration of the cells was controlled so that the substrate has coverage of around 10^5 yeast cells/cm^2.

Sample Preparation for SEM Imaging. Prior to SEM imaging, cell culture is fixed in mixed primary fixative (3% paraformaldehyde/0.1 M sodium cacodylate/0.05 M $CaCl_2$/0.05 M $MgCl_2$/2.5% sucrose and 1.5% glutaraldehyde at pH 7.4) at room temperature for 1 h, then rinsed three times with 0.1 M sodium cacodylate/2.5% sucrose solution. The cell culture is subsequently treated with postfixative of 1% osmium tetraoxide in 0.1 M cacodylate buffer at pH 7.4 on ice for 1 h, and then rinsed thoroughly with water, and dehydrated with grade series of cold ethanol (70, 90, 100%). The sample was then dried in a critical point dryer and coated with 60 nm carbon for SEM imaging.

Acknowledgment. This work was supported by a grant from the Volkswagen Foundation (I/84 072). Authors thank for fruitful discussions D. Makarov, L. Baraban, A. Ananth, and V. Gupta. Authors thank C. Krien and R. Engelhard for technical support, S. Baunack for help with SEM, and D. Grimm for clean room support. A.S. thanks Y. Mei. for discussions. D.G. acknowledges financial support from Alexander von Humboldt Foundation.

Supporting Information Available: Additional experimental details of the fabrication of tubes and videos of self-propelled nanotools are included. This material is available free of charge *via* the Internet at http://pubs.acs.org.

REFERENCES AND NOTES

1. Feynman, R. P. There's Plenty of Room at the Bottom. *J. Microelectromech. Syst.* **1992**, *1*, 60–66.
2. Mallouk, T. E.; Sen, A. Powering Nanorobots. *Sci. Am.* **2009**, *300*, 72–77.
3. Ismagilov, R. F.; Schwartz, A.; Bowden, N.; Whitesides, G. M. Autonomous Movement and Self-Assembly. *Angew. Chem., Int. Ed.* **2002**, *41*, 652–654.
4. Paxton, W. F.; Kistler, K. C.; Olmeda, C. C.; Sen, A.; St. Angelo, S. K.; Cao, Y.; Mallouk, T. E.; Lammert, P. E.; Crespi, V. H.

Catalytic Nanomotors: Autonomous Movement of Striped Nanorods. *J. Am. Chem. Soc.* **2004**, *126*, 13424–13431.
5. Dhar, P.; Fischer, T. M.; Wang, Y.; Mallouk, T. E.; Paxton, W. F.; Sen, A. Autonomously Moving Nanorods at a Viscous Interface. *Nano Lett.* **2006**, *6*, 66–72.
6. Ozin, G. A.; Manners, I.; Fournier-Bidoz, S.; Arsenault, A. Dream Nanomachines. *Adv. Mater.* **2005**, *17*, 3011–3018.
7. Paxton, W. F.; Sundararajan, S.; Mallouk, T. E.; Sen, A. Chemical Locomotion. *Angew. Chem., Int. Ed.* **2006**, *45*, 5420–5429.
8. Mirkovic, T.; Zacharia, N. S.; Scholes, G. D.; Ozin, G. A. Nanolocomotion- Catalytic Nanomotors and Nanorotors. *Small* **2010**, *6*, 159–167.
9. Pumera, M. Electrochemically Powered Self-Propelled Electrophoretic Nanosubmarines. *Nanoscale* **2010**, *2*, 1643–1649.
10. Sanchez, S.; Pumera, M. Nanorobots: The Ultimate Wireless Self-Propelled Sensing and Actuating Devices. *Chem.—Asian J.* **2009**, *4*, 1402.
11. Pumera, M. Nanomaterials Meet Microfluidics. *Chem. Commun.* **2011**, *47*, 5637–5904.
12. Laocharoensuk, R.; Burdick, J.; Wang, J. CNT-Induced Acceleration of Catalytic Nanomotors. *ACS Nano* **2008**, *2*, 1069–1075.
13. Ebbens, S. J.; Howse, J. R. Direct Observation of the Direction of Motion for Spherical Catalytic Swimmers. *Langmuir* **2011**, *27*, 12293–12296.
14. Baraban, L.; Tasinkevych, M.; Popescu, M. N.; Sanchez, S.; Dietrich, S.; Schmidt, O. G. Transport of Cargo by Catalytic Janus Micro-Motors. *Soft Matter* **2012**, *8*, 48–52.
15. Howse, J. R.; Jones, R. A. L.; Ryan, A. J.; Gough, T.; Vafabakhsh, R.; Golestanian, R. Self-Motile Colloidal Particles: From Directed Propulsion to Random Walk. *Phys. Rev. Lett.* **2007**, *99*, 048102.
16. Paxton, W. F.; Baker, P. T.; Kline, T. R.; Wang, Y.; Mallouk, T. E.; Sen, A. Catalytically Induced Electrokinetics for Motors and Micropumps. *J. Am. Chem. Soc.* **2006**, *128*, 14881–14888.
17. Ibele, M. E.; Wang, Y.; Kline, T. R.; Mallouk, T. E.; Sen, A. Hydrazine Fuels for Bimetallic Catalytic Microfluidic Pumping. *J. Am. Chem. Soc.* **2007**, *129*, 7762–7763.
18. Solovev, A. A.; Sanchez, S.; Mei, Y. F.; Schmidt, O. G. Tunable Catalytic Tubular Micro-Pumps Operating at Low Concentrations of Hydrogen Peroxide. *Phys. Chem. Chem. Phys.* **2011**, *13*, 10131–10135.
19. Sundararajan, S.; Lammert, P. E.; Zudans, A. W.; Crespi, V. H.; Sen, A. Catalytic Motors for Transport of Colloidal Cargo. *Nano Lett.* **2008**, *8*, 1271–12765.
20. Burdick, J.; Laocharoensuk, R.; Wheat, P. M.; Posner, J. D.; Wang, J. Synthetic Nanomotors in Microchannel Networks: Directional Microchip Motion and Controlled Manipulation of Cargo. *J. Am. Chem. Soc.* **2008**, *130*, 8164–8165.
21. Schmidt, O. G.; Eberl, K. Thin Solid Films Roll Up into Nanotubes. *Nature* **2001**, *410*, 168.
22. Golod, S. V.; Prinz, V. Ya.; Waegli, P.; Zhang, L.; Kirfel, O.; Deckardt, E.; Glaus, F.; David, C.; Grützmacher, D. Free-standing SiGe/Si/Cr and SiGe/Si/SixNy/Cr Microtubes. *Appl. Phys. Lett.* **2004**, *84*, 3391.
23. Tyagi, P.; Bassik, N.; Leong, T. G.; Cho, J. H.; Benson, B. R.; Gracias, D. H. Self-Assembly Based on Chromium/Copper Bilayers. *J. Microelectromech. Syst.* **2009**, *18*, 784–791.
24. Mei, Y. F.; Huang, G. S.; Solovev, A. A.; Ureña, E. B.; Mönch, I.; Ding, F.; Reindl, T.; Fu, R. K. Y.; Chu, P. K.; Schmidt, O. G. Versatile Approach for Integrative and Functionalized Tubes by Strain Engineering of Nanomembranes on Polymers. *Adv. Mater.* **2008**, *20*, 4085–4090.
25. Bof' Bufon, C. C.; Cojal Gonzalez, J. D.; Thurmer, D. J.; Grimm, D.; Bauer, M.; Schmidt, O. G. Self-Assembled Ultra-Compact Energy Storage Elements Based on Hybrid Nanomembranes. *Nano Lett.* **2010**, *10*, 2506–2510.
26. Solovev, A. A.; Mei, Y. F.; Ureña, E. B.; Huang, G.; Schmidt, O. G. Catalytic Microtubular Jet Engines Self-Propelled by Accumulated Gas Bubbles. *Small* **2009**, *5*, 1688–1692.
27. Mei, Y. F.; Solovev, A. A.; Sanchez, S.; Schmidt, O. G. Rolled-Up Nanotech on Polymers: From Basic Perception to Self-Propelled Catalytic Microengines. *Chem. Soc. Rev.* **2011**, *40*, 2109–2119.
28. Solovev, A. A.; Smith, E. J.; Bof' Bufon, C. C.; Sanchez, S.; Schmidt, O. G. Light-Controlled Propulsion of Catalytic Microengines. *Angew. Chem., Int. Ed.* **2011**, *50*, 10875–10878.
29. Sanchez, S.; Ananth, A. N.; Fomin, V. M.; Viehrig, M.; Schmidt, O. G. Superfast Motion of Catalytic Microjet Engines at Physiological Temperature. *J. Am. Chem. Soc.* **2011**, *133*, 14860–14863.
30. Solovev, A. A.; Sanchez, S.; Pumera, M.; Mei, Y. F.; Schmidt, O. G. Magnetic Control of Tubular Catalytic Microbots for the Transport, Assembly and Delivery of Micro-Objects. *Adv. Funct. Mater.* **2010**, *20*, 2430–2435.
31. Sanchez, S.; Solovev, A. A.; Harazim, S. M.; Schmidt, O. G. Microbots Swimming in the Flowing Streams of Microfluidic Channels. *J. Am. Chem. Soc.* **2011**, *133*, 1131–1134.
32. Sanchez, S.; Solovev, A. A.; Schulze, S.; Schmidt, O. G. Controlled Manipulation of Multiple Cells Using Catalytic Microbots. *Chem. Commun.* **2011**, *47*, 698–700.
33. Balasubramanian, S.; Kagan, D.; Hu, C.-M. J.; Campuzano, S.; Lobo-Castañon, M. J.; Lim, N.; Kang, D. Y.; Zimmerman, M.; Zhang, L.; Wang, J. Micromachine-Enabled Capture and Isolation of Cancer Cells in Complex Media. *Angew. Chem., Int. Ed.* **2011**, *123*, 4247–4250.
34. Kagan, D.; Campuzano, S.; Balasubramanian, S.; Kuralay, F.; Flechsig, G.-U.; Wang, J. Functionalized Micromachines for Selective and Rapid Isolation of Nucleic Acid Targets from Complex Samples. *Nano Lett.* **2011**, *11*, 2083–2087.
35. Sanchez, S.; Solovev, A. A.; Harazim, S. M.; Deneke, C.; Mei, Y. F.; Schmidt, O. G. The Smallest Man-Made Jet Engine. *Chem. Rec.* **2011**, *11*, 367–370.
36. http://www.guinnessworldrecords.com/records-9000/smallest-jet-engine/
37. Prinz, V. Ya.; Seleznev, V. A.; Gutakovsky, A. K.; Chehovskiy, A. V.; Preobrazenskii, V. V.; Putyato, M. A.; Gavrilova, T. A. Low-Dimensional Systems and Nanostructures. *Physica E* **2000**, *6*, 828–831.
38. Deneke, Ch.; Müller, C.; Jin-Phillipp, N. Y.; Schmidt, O. G. Diameter Scalability of Rolled-Up In(Ga)As/GaAs Nanotubes. *Semicond. Sci. Technol.* **2002**, *17*, 1278–1281.
39. Nikishkov, G. P. Curvature Estimation for Multilayer Hinged Structures with Initial Strains. *J. Appl. Phys.* **2003**, *94*, 5333–5336.
40. Grundmann, M. Nanoscroll Formation from Strained Layer Heterostructures. *Appl. Phys. Lett.* **2003**, *83*, 2444–2446.
41. Deneke, C.; Sigle, W.; Eigenthaler, U.; van Aken, P. A.; Shütz, G.; Schmidt, O. G. Interfaces in Semiconductor/Metal Radial Superlattices. *Appl. Phys. Lett.* **2007**, *90*, 263107.
42. Purcell, E. M. Life at Low Reynolds Number. *Am. J. Phys.* **1977**, *45*, 3–11.
43. Soap composition: 5−15% anionic tenside (5−15%), amphoteric tenside (<5%), bronopol, benzisothiazolinone, methylisothiazolinone.
44. Harazim, S. M.; Feng, P.; Sanchez, S.; Deneke, C.; Mei, Y. F.; Schmidt, O. G. Integrated Sensitive On-Chip Ion Field Effect Transistors Based on Wrinkled InGaAs Nanomembranes. *Nanoscale Res. Lett.* **2011**, *6*, 215.
45. Pantarotto, D.; Browne, W. R.; Feringa, B. L. Autonomous Propulsion of Carbon Nanotubes Powered by a Multienzyme Ensemble. *Chem. Commun.* **2008**, 1533–1535.
46. Mano, N.; Heller, A. Bioelectrochemical Propulsion. *J. Am. Chem. Soc.* **2005**, *127*, 11574–11575.
47. Sanchez, S.; Solovev, A. A.; Mei, Y. F.; Schmidt, O. G. Dynamics of Biocatalytic Microengines Mediated by Variable Friction Control. *J. Am. Chem. Soc.* **2010**, *132*, 13144–13145.
48. Solovev, A. A.; Smith, E. J.; Bof' Bufon, C. C.; Sanchez, S.; Schmidt, O. G. Light-Controlled Propulsion of Catalytic Microengines. *Angew. Chem., Int. Ed.* **2011**, *50*, 10875–10878.
49. Hong, Y.; Blackman, N. M. K.; Kopp, N. D.; Sen, A.; Velegol, D. Chemotaxis of Nonbiological Colloidal Rods. *Phys. Rev. Lett.* **2007**, *99*, 178103.
50. Calvo-Marzal, P.; Manesh, K. M.; Kagan, D.; Balasubramanian, S.; Cardona, M.; Flechsig, G.-U.; Posner, J.; Wang, J. Electrochemically-Triggered Motion of Catalytic Nanomotors. *Chem. Commun.* **2009**, 4509.